Solar Physics
DOI: 10.1007/•••••-•••-•••-••••-•

Two-Dimensional Power, Phase, and Coherence Spectra of Solar Dynamics Observatory Helioseismic Observables

Rachel Howe[1] · **Kiran Jain**[2] · **Richard S Bogart**[3] · **Deborah A Haber**[4] · **Charles S Baldner**[3]

Abstract While the Helioseismic and Magnetic Imager [HMI] aboard the Solar Dynamics Observatory [SDO] provides Doppler velocity [V], continuum intensity [I_C] and line depth observations, each of which is sensitive to the 5-minute acoustic spectrum, the Atmospheric Imaging Array [AIA] also observes at wavelengths — specifically the 1600 and 1700 Angstrom bands — that are formed in the upper photosphere and have good sensitivity to acoustic modes. In this paper we consider the characteristics of the acoustic spectra in AIA and HMI observables for a 15-degree region around active region NOAA 11072. We map the acoustic power distribution for the different observables and the HMI Line Core (Continuum minus Line Depth) and the phase and coherence functions for selected observable pairs, as a function of position and frequency. Five-minute power in all observables is suppressed in the sunspot and also in plage areas. Above the acoustic cut off frequency the behaviour is more complicated: power in HMI I_C is still suppressed in the presence of surface magnetic fields, while power in HMI I_L and the AIA bands is suppressed in areas of surface field but enhanced in an extended area around the active region, and power in HMI V is enhanced in a narrow zone around strong field concentrations and suppressed in a wider surrounding area. The relative phase of the observables, and their cross-coherence functions, are also altered around the active region. These effects may help us to understand the interaction of waves and magnetic fields in the different layers of the photosphere, and will need to be taken into account in multi-wavelength local helioseismic analysis of active regions.

Keywords: Helioseismology, Chromospheric oscillations, Ultraviolet observations, Magnetic fields, Active regions, Acoustic power maps

[1] School of Physics and Astronomy, University of Birmingham, Edgbaston, Birmingham B15 2TT, UK email: rhowe@noao.edu
[2]National Solar Observatory, 950 N. Cherry Avenue, Tucson AZ 85719, USA
[3]Stanford University, Stanford, CA 94305-4085, USA
[4]JILA, University of Colorado, Boulder, CO, USA

1. Introduction

Helioseismology relies on the observation of waves, as they affect light from the outer layers of the Sun, to infer the structure and dynamics of the otherwise invisible deeper layers. By studying the oscillations in multiple wavelengths of light — and hence at different heights in the atmosphere — simultaneously, it is possible to probe the layers of the atmosphere. Such investigations, aiming both to better understand the behaviour of the waves and their interaction with magnetic fields, and to improve the inference of subsurface properties, have a long history.

The launch in February 2010 of the Solar Dynamics Observatory [SDO], carrying both the Helioseismic and Magnetic Imager [HMI] and the Atmospheric Imaging Assembly [AIA], provides new opportunities for cross-spectral helioseismic analysis, with full-disc, high-cadence images at many UV and EUV wavelengths from AIA as well as photospheric Doppler velocity, continuum and magnetic data from HMI. As discussed by Howe *et al.* (2011), who considered the Sun-as-a-star spectra from the AIA and HMI observables, the AIA 1600 Å and 1700 Å near-ultraviolet bands show a clear signature of the five-minute acoustic spectrum that is much less contaminated by granulation "noise" than the continuum intensity in HMI's visible 6173 Å line.

Both the effect of surface magnetic activity on helioseismic waves in local areas, and the phase and coherence relationships between the velocity and the intensity of radiation at different wavelengths (and hence from different heights in the solar atmosphere), have been studied for nearly two decades.

Brown *et al.* (1992) reported finding small areas associated with active regions that produced a disproportionate amount of acoustic power in the 5.5 – 7.5 mHz frequency band in ground-based Doppler observations using the Fe I 5576 Å line, while Braun *et al.* (1992) made the first observations of clear acoustic haloes around active regions in the same frequency band using Ca K intensity. However, atmospheric seeing can have confusing effects on ground-based intensity observations (Hill *et al.*, 2001). The picture became clearer with the launch of the Michelson Doppler Imager [MDI] (Scherrer *et al.*, 1995) aboard the Solar and Heliospheric Observatory [*SOHO*], which allowed full-disk observations from space in both intensity and velocity using the 6768 Å Ni line. Jain and Haber (2002) studied the power distribution in the line depth, Doppler velocity, and continuum intensity observables from MDI. In both sunspot and plage regions they found that the power in areas of strong magnetic field was suppressed in all observables, while for velocity and line depth (but not for continuum intensity) there was a "halo" of enhanced power surrounding the magnetic field concentrations, which they concluded was acoustic in origin. The Transition Region and Coronal Observer [TRACE] made possible high-resolution, space-based observations in the 1600 and 1700 Å bands. Judge, Tarbell, and Wilhelm (2001) used data from another *SOHO* instrument, SUMER (Solar Ultraviolet Measurements of Emitted Radiation), TRACE, and MDI to investigate the oscillations in the chromosphere. This work established for the first time that the chromospheric modes were primarily the same p modes seen in the photosphere. Krijger *et al.* (2001) used TRACE to study oscillations in the 1600 Å UV band in quiet Sun

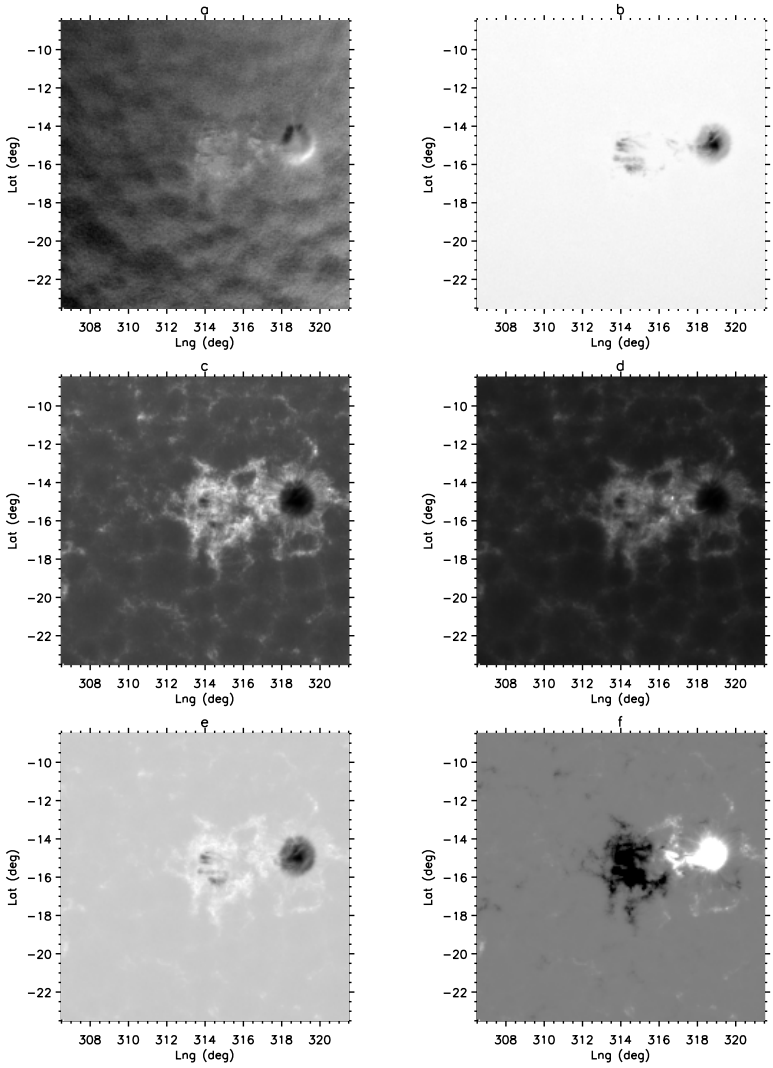

Figure 1. Mean values of each observable for 2010 May 23: HMI V (a), HMI I_C (b), AIA 1600 (c), AIA 1700 (d), HMI I_L (e), and HMI longitudinal magnetic field strength (f).

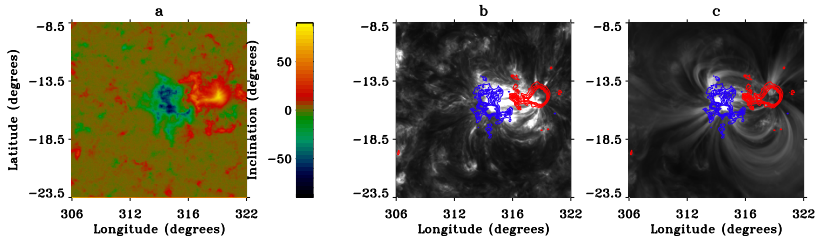

Figure 2. The mean magnetic inclination (a), courtesy K. Hayashi, an AIA 304 Å image (b) and an AIA 171 Å image (c), for the area of interest on 2010 May 23. The contours overlaid on panels a and b show the mean magnetic field strength with contours at 100G intervals.

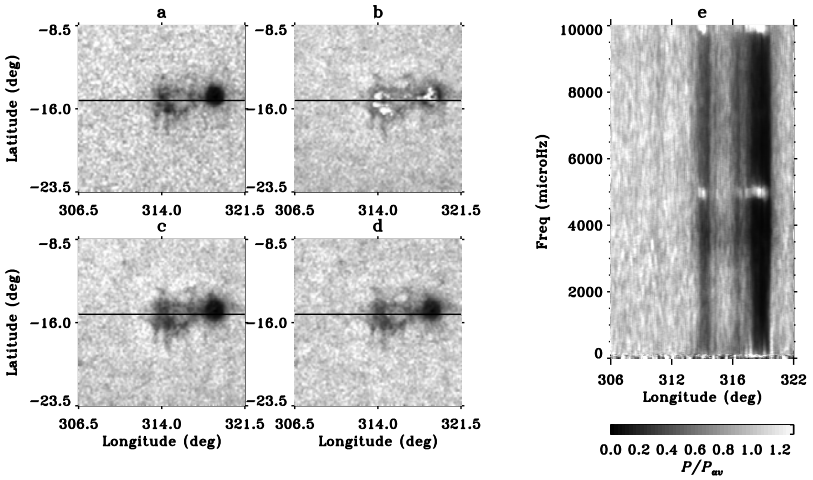

Figure 3. Slices through the smoothed relative-power maps for HMI I_C, at 3 mHz (a), 5 mHz (b), 7 mHz (c), 9 mHz (d), and in longitude and temporal frequency along the horizontal line shown in panels a-d (e).

and found enhanced power at 3-minute periods around patches of network field. Muglach (2003) also looked at acoustic power around an active region in short (2 – 4 hour) stretches of TRACE data and did not find a high-frequency acoustic halo in the 1600 or 1700 Å bands.

Schunker and Braun (2011) have examined the power distribution for velocity observations from MDI and found that the excess high-frequency power corresponds to regions with the magnetic field inclination (as deduced from potential-field source-surface extrapolation) in the 40 – 60 degree range. However, the exact origin of these high-frequency haloes remains unclear.

The relative phase of the Doppler velocity and the intensity in various wavelength bands has been studied for more than two decades in both resolved and unresolved observations. Early (ground-based) spatially-resolved phase measurements were made, for example, by Deubner *et al.* (1990, 1992); in the latter paper they used three different wavelengths including the Na D line, formed in the lower chromosphere. These measurements revealed a complicated pattern of phase relationships that was not easily explained by simple models. Moretti *et al.* (2007) made ground-based observations from the South Pole using the MOTH instrument (Finsterle *et al.*, 2004), taking high-cadence images in the Sodium and Potassium D-lines. The Sodium line shows clear evidence of a high-frequency halo around an active region.

In this paper we will examine the behaviour and relationships of the different observables in a small region of the solar surface containing an active region as observed by HMI and AIA, and show how the power and phase of the oscillations is affected by the presence of local magnetic fields. For this purpose we will show observations of NOAA active region 11072 on 23 May 2010. We have also examined the data for the same region over the two preceding and following days; the results are very similar and for reasons of space are not shown in this paper.

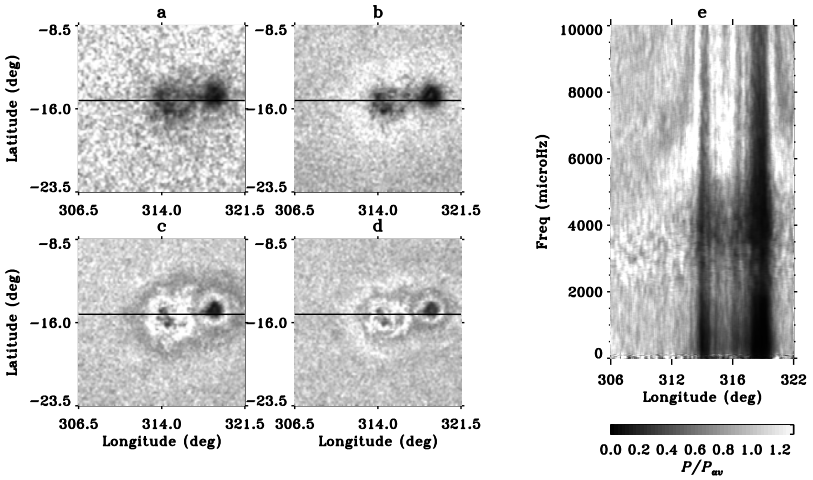

Figure 4. Slices through the smoothed relative-power maps for HMI V at 3 mHz (a), 5 mHz (b), 7 mHz (c), 9 mHz (d), and in longitude and temporal frequency along the horizontal line shown in panels a-d (e).

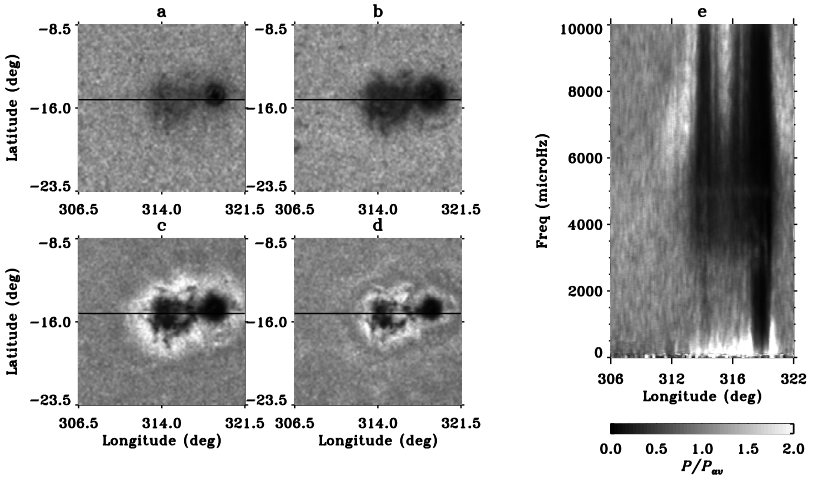

Figure 5. Slices through the smoothed relative-power maps for HMI I_L, at 3 mHz (a), 5 mHz (b), 7 mHz (c), 9 mHz (d), and in longitude and temporal frequency along the horizontal line shown in panels a-d (e).

In section 2 we will describe our data and analysis and define the phase and coherence spectra. In section 3 we show the region in each of the observables; in section 4 we present the power maps for each observable, and in section 5 we show the phase and coherence spectra. In section 6 we discuss our findings.

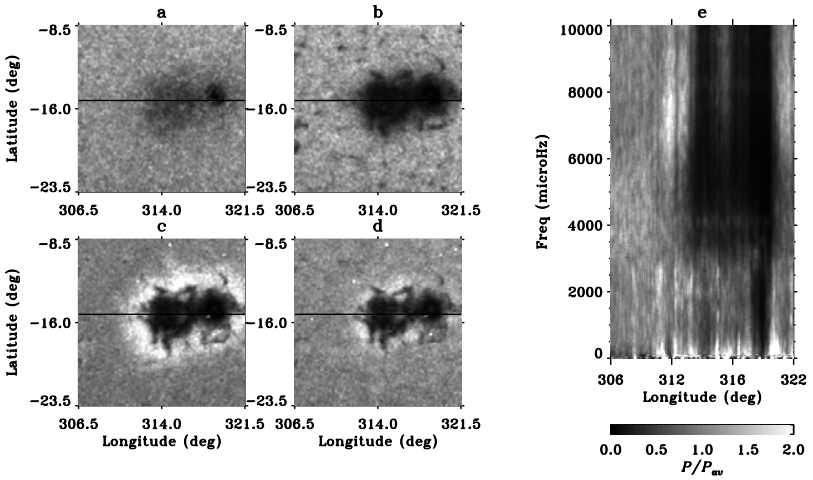

Figure 6. Slices through the smoothed relative-power maps for AIA 1700, at 3 mHz (a), 5 mHz (b), 7 mHz (c), 9 mHz (d), and in longitude and temporal frequency along the horizontal line shown in panels a-d (e).

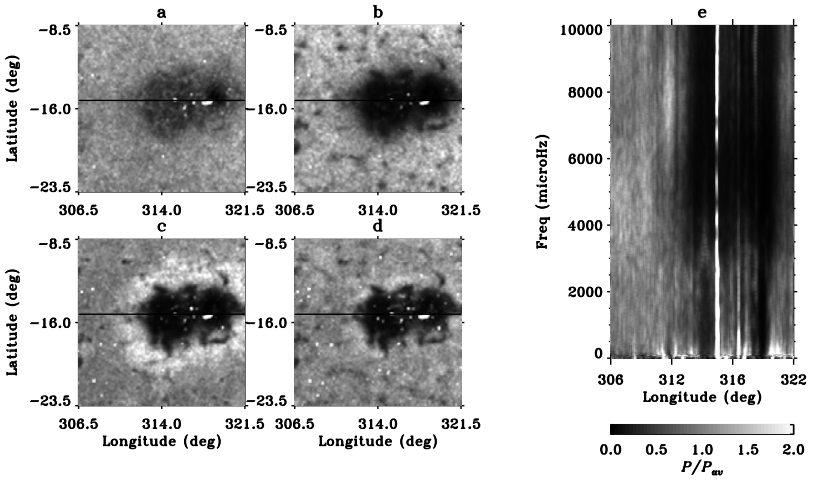

Figure 7. Slices through the smoothed relative-power maps for AIA 1600, at 3 mHz (a), 5 mHz (b), 7 mHz (c), 9 mHz (d), and in longitude and temporal frequency along the horizontal line shown in panels a-d (e).

2. Data and Analysis

2.1. Helioseismic Observables from the Solar Dynamics Observatory

The HMI observables are produced from observations of the Fe I line at 6173 Å by combining "filtergrams" taken with different configurations of the instrument's filters. For each 45-second interval there is a line-of-sight magnetogram, a Doppler velocity image [HMI V], a continuum intensity image [HMI I_C], a Line Depth image [HMI Ld] and also a Line Width image, which is not considered

here. For this investigation we consider the HMI I_C and HMI V observables and also a Line Core intensity observable [Hmi I_L] formed by taking the difference between HMI I_C and HMI Ld. The resolution of the 4096×4096 pixel images is approximately 0.5 arcsec.

Norton *et al.* (2006) found that the height of formation of the HMI 6173 Å line spans the range from 20 km at the wings to 270 km at the core. Fleck, Couvidat, and Straus (2011) have calculated that the height of formation of the HMI Doppler velocity is approximately 100 km, slightly lower than that of the Ni 6768 Å line used by MDI. However, the finite resolution of the instruments raises the effective height of formation by about 50 km at disk centre in both cases. We can therefore say that the HMI I_C observable is formed considerably lower in the atmosphere than HMI I_L, with HMI V at an intermediate depth.

The AIA 1600 Å images for the day analyzed have a cadence of 24 s, while the cadence for 1700 Å was 48 seconds. (More recent data have used a consistent 24s cadence for both, but the cadences were adjusted several times during the early months of AIA observations.) These images are also taken at 4096×4096 pixels, but because AIA allows more room around the limb of the solar image the resolution is approximately 0.6 arcsec. The 1700 Å band is believed to be formed in the upper photosphere; Judge, Tarbell, and Wilhelm (2001) put it at $300-550$ km, around the temperature minimum between the upper photosphere and lower chromosphere. The 1600 Å band includes the C IV line and samples both the transition region at the top of the chromosphere and the upper photosphere. The calculations of Fossum and Carlsson (2005) for the equivalent TRACE bandpasses give mean formation heights of 360 km and 480 km for the 1700 and 1600 Å bands, with FWHM of 385 and 185 km respectively; these authors also note that the passbands are double peaked, with the 1700 Å in particular having two almost equal components centered at 402 ± 259 and 208 ± 174 km. The helioseismic signal in the 1600 Å band, therefore, is in general somewhat contaminated by flare activity, but there are no strong flares during the day analysed. It seems unlikely that the strong global p-mode signal found by Howe *et al.* (2011) in both 1600 Å and 1700 Å bands could originate as high as the transition region, and we therefore suspect that the helioseismic response in this bandpass is associated with the continuum rather than the C IV line and pertains to a height range not very far above that involved in the 1700 Å band. We should note that the calibration and registration of the AIA data are less thorough than for the HMI data, so there is a possibility of position errors and small drifts, of the order of a fraction of a pixel over several days, which could affect comparisons at the pixel level but should not be a serious problem for the analysis described here, which involves smoothing over several detector pixels.

The data were obtained from the JSOC web site, http://jsoc.stanford.edu/. The website allows the extraction of a "tracked hg_patch" from each image; these patches can be chosen to be centred on a given heliographic location but are not remapped. For each observable we obtained a 24-hour sequence of such patches centred on the location of AR 11072, covering the whole of 2010 May 23. These patches were based on images from the aia.lev1 series and the (level 1.5) series hmi.V_45s, hmi.Ic_45s and hmi.Ld_45s; these are the most final calibrations of the data available at the time of writing. The data were then remapped to a

common 201×201 pixel grid, 15 heliographic degrees on each side, evenly spaced in heliographic latitude and longitude, and interpolated to a uniform 45 second cadence. A running mean over 15 minutes was subtracted from each remapped pixel time series to remove effects such as daily variations due to the orbit of SDO.

2.2. Phase and Coherence Functions

The relationship between two time series in the Fourier domain can be expressed in terms of the cross-spectrum, the phase difference, and the cross-coherence, which we define as follows.

Let $P_A(\nu)$ and $P_B(\nu)$ be the complex Fourier spectra of two time series. The "cross spectrum" is defined as

$$\mathrm{CROSS}(\nu) \equiv P_{AB} = P_A(\nu) \cdot P_B^*(\nu) \tag{1}$$

The phase difference $\delta\phi_{A,B}$ can be written as

$$\delta\phi_{AB}(\nu) = \arg\langle P_{AB}(\nu)\rangle. \tag{2}$$

We adopt the convention that a positive value of $\delta\phi_{AB}$ means that A leads B.

The coherence spectrum, a measure of the correlation of the two spectra as a function of frequency, can be written as

$$\mathrm{COH_{AB}}(\nu) = \frac{|\langle P_{AB}(\nu)\rangle|}{\sqrt{\langle|P_A(\nu)|^2\rangle\langle|P_B(\nu)|^2\rangle}}. \tag{3}$$

The angle brackets formally denote the expectation value; in practice this can be approximated by a mean over many short spectra as in the work of Elsworth *et al.* (1994), a smoothing by a running mean in the frequency domain, as used by Jiménez *et al.* (1999), or, for resolved-Sun observations (Severino *et al.*, 2001; Barban, Hill, and Kras, 2004) an average over all azimuthal orders m for a given degree l. For a finite amount of data these approximations may give slightly different results. In the present work we use a 3-dimensional boxcar smoothing of the data cube of one-dimensional power spectra, smoothing over 3 remapped pixels in the spatial direction and 0.3 mHz in temporal frequency.

3. Images

In Figure 1 we show the mean image for each of the observables for 2010 May 23. On this date the active region was somewhat mature, with a well-defined leading spot and a following-polarity region consisting mostly of strong plage with a couple of small sunspots, and was close to the central meridian. In the Doppler velocity panel the supergranulation is clearly visible; the active region disrupts the supergranular pattern and produces the familiar artifactual appearance of an upflow on one side of the penumbra and a downflow on the other. The sunspot umbra and penumbra show as darkened areas in all the intensity observables, but

the weaker fields in the following–polarity region and surrounding network are bright in the AIA bands and in HMI I_L. The network fields clearly correspond to the supergranule boundaries. For additional context, we show in Figure 2 the mean magnetic field inclination from Milne-Eddington inversions of HMI magnetograms and the AIA images at 304 and 171 Å, which show the structure of the overlying coronal loops that connect the leading and following regions.

4. Power Maps

In order to study the local power distribution in each observable, we calculated the power spectrum in each pixel of the remapped data cubes. The spectra were then smoothed over 25 bins (about 0.3 mHz) in temporal frequency and three bins in each spatial direction, and the power at each frequency was normalized by the mean power for that frequency across the whole data cube.

We now examine the power maps for each observable in turn, taking them in ascending order of height of formation.

4.1. HMI I_C

Figure 3 shows four sample relative power maps at 3, 5, 7, and 9 mHz and a slice through the stack of relative power maps at constant latitude passing through the body of the active region, for the HMI I_C data cube. The acoustic cut-off frequency in quiet Sun is around 5mHz. In this case, and for all the other intensity observables, we divided each time series by the mean intensity for the pixel to remove the unwanted effects of brighter regions. Power is suppressed in the active region at all frequencies; there is very little variation in the pattern of power suppression with frequency, though there is slightly stronger suppression in the five-minute band and above than in the granulation (≤ 2.5 mHz) range. There is no sign of any haloes of excess power. The narrow spike of excess power within the sunspot around 5mHz is seen in only one of the other four days examined and may be a noise artifact. The power map shows somewhat finer detail at higher frequencies, presumably due to the way that the low-frequency limit of the p-mode spectrum at the f-mode ridge shifts towards higher spatial frequencies with increasing temporal frequency.

4.2. HMI Velocity

In Figure 4 we show the results for the HMI V power. Here we see the well-known suppression of the acoustic power in the active region in the five-minute frequency band, and a weak, broad halo of excess power surrounding the active region at 5 mHz. In the 7 mHz band the excess power has shrunk to a narrow belt outlining the active region and surrounded by a wider region of suppressed power, with a hint of a more diffuse enhancement beyond that. At this frequency, the suppression of power within the sunspot is much weaker and even cancelled out by the enhancement around the edges. Examination of the longitude-frequency slice suggests that the halo of enhanced power contracts towards the active region with increasing frequency..

4.3. HMI I_L

Figure 5 shows slices through the power maps for HMI I_L. Here, there is a strong halo of excess power — so strong that we have used a wider greyscale range than for the I_C and V maps — above about 6 mHz surrounding the active region, but farther out than that seen in the velocity observations. This region is beyond that where there is any detectable concentration of surface magnetic field, and has no obvious correspondence to the morphology of the overlying magnetic loops as revealed in the AIA 304 Å and 171 Å images. At 7 mHz, it occupies about the same area as the outer band of reduced power in the velocity power map. Within the halo, there are "tendrils" of power suppression that correspond to concentrations of plage field, giving it a patchy appearance. As in the velocity observations, this halo appears to contract with increasing frequency, and at 9 mHz it has collapsed to a narrow band around the sunspots, much the same as that seen in the HMI V at 7 mHz. The existence of the halo is consistent with the findings of Jain and Haber (2002), who saw a similar phenomenon in the MDI line depth observations.

4.4. AIA 1700 and 1600

Finally, we show the power-map slices for AIA 1700 (Figure 6) and AIA 1600 (Figure 7). As in HMI I_L, the power in the active region is more strongly suppressed at 5 mHz than in the five-minute band, and suppression is also visible for weak network field concentrations in the quiet Sun. Also as seen in HMI I_L, there is an outlying halo of high-frequency excess power surrounding the active region. This appears to contradict the findings of Muglach (2003), who did not find any excess power in these bands in TRACE observations. However, we reiterate that this power excess is at a greater distance from the active region than the halo in velocity, and also occurs at higher temporal frequencies. Haloes of excess power have also been seen in ground-based observations using chromospheric lines, for example by Moretti *et al.* (2007) in the Na D line and by Braun *et al.* (1992) in Ca K. The halo region contracts and weakens with increasing frequency, becoming indistinct by about 10 mHz, but the collapse and encroachment on the active region seen in the HMI V and HMI I_L cases do not happen up to the 10.4 mHz Nyquist frequency of the 1700 Å data set, and a re-analysis of the 1600 Å data with the full 24 s temporal resolution did not reveal any such effect at higher frequencies.

5. 2-dimensional phase and coherence maps

The phase and coherence of the individual remapped pixel time series, as a function of position and frequency, can be derived using Eq. 2 and Eq. 3. When the coherence is low there is little relationship between the two signals and we can expect the apparent phase difference to be close to zero after spatial averaging.

In Figures 8 to 15 we show these quantities for the combination of HMI V with HMI I_C, HMI I_L, AIA 1700, and AIA 1600. The velocity is treated as positive in

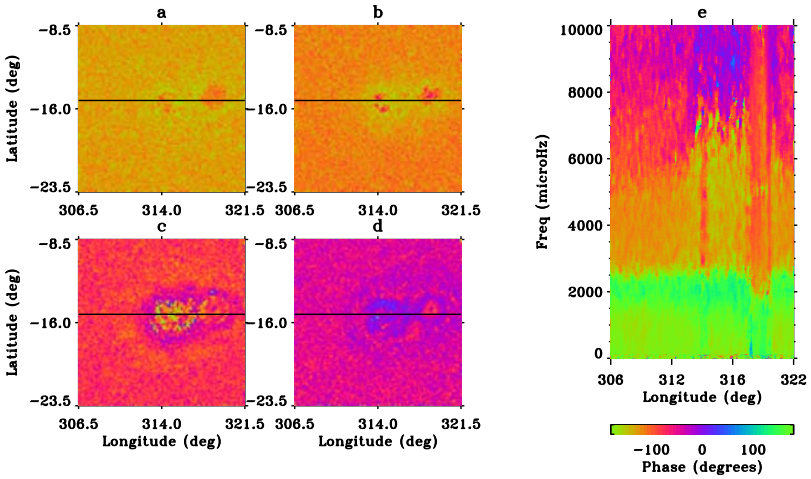

Figure 8. Slices through the HMI I_C/HMI V phase, at 3 mHz (a), 5 mHz (b), 7 mHz (c), 9 mHz (d), and in longitude and temporal frequency along the horizontal line shown in panels a-d (e).

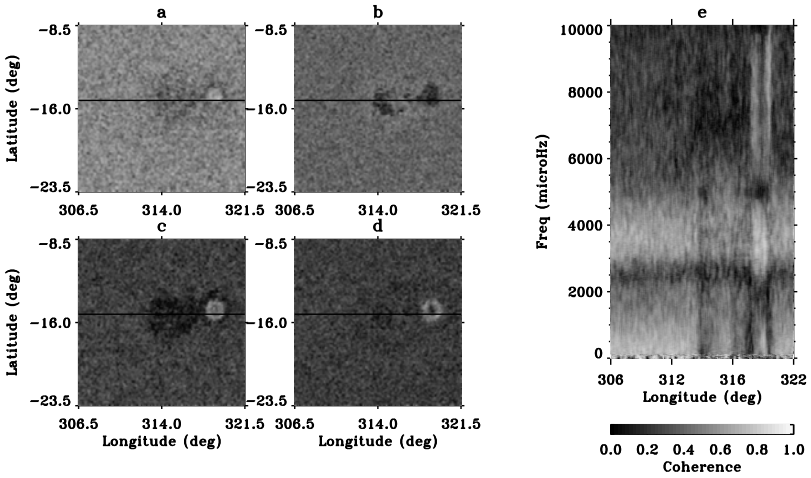

Figure 9. Slices through the HMI I_C/HMI V coherence, at 3 mHz (a), 5 mHz (b), 7 mHz (c), 9 mHz (d), and in longitude and temporal frequency along the horizontal line shown in panels a-d (e).

the direction away from the observer. In all cases, the coherence with the velocity is sharply reduced within the active region, which is understandable due to the greatly reduced mode power and consequent reduction in signal-to-noise ratio. There is, however, a local increase in coherence in the core of the sunspot for all three cases. This may be a real effect, but we should be cautious of common spurious, or at least complicating, effects within the sunspot umbra, such as noise interacting with the steep gradients of power and intensity, contamination by other spectral lines due to reduced temperatures, and possible cross-talk between the HMI observables in the presence of strong fields.

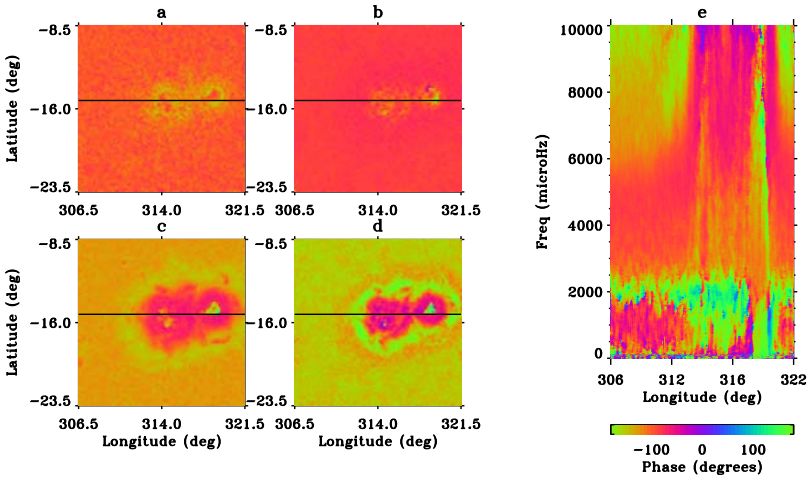

Figure 10. Slices through the HMI I_L/HMI V phase, at 3 mHz (a), 5 mHz (b), 7 mHz (c), 9 mHz (d), and in longitude and temporal frequency along the horizontal line shown in panels a-d (e).

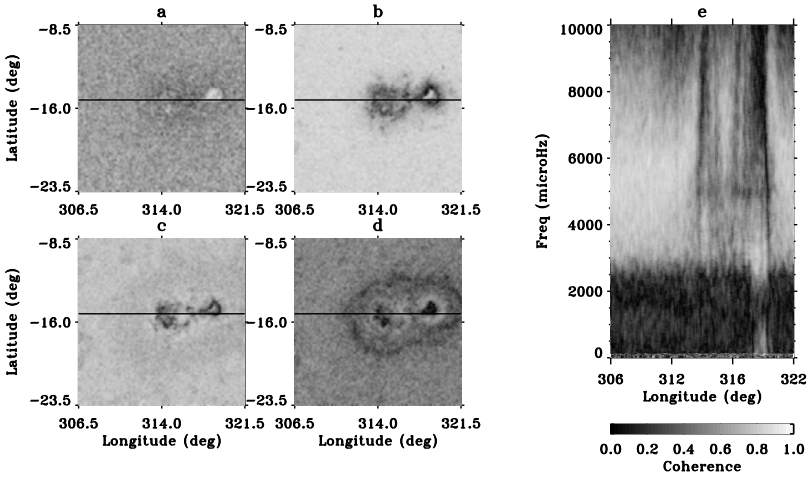

Figure 11. Slices through the HMI I_L/HMI V coherence at 3 mHz (a), 5 mHz (b), 7 mHz (c), 9 mHz (d), and in longitude and temporal frequency along the horizontal line shown in panels a-d (e).

The phase difference between HMI V and HMI I_C shows a sharp discontinuity at around 2.5 mHz, the upper limit of the granulation signal; this phenomenon has been well known since the work of, for example, Staiger (1985) as illustrated by Deubner *et al.* (1990), Deubner *et al.* (1990) and Jiménez *et al.* (1999). In the core of the active region this boundary is shifted to lower frequencies, perhaps due to the suppression of convective motions by the surface fields. The weaker fields of the plage area have very little effect on the I – V phase in the five-minute band, but do modulate the HMI I_L – HMI V phase difference. In the HMI I_L and

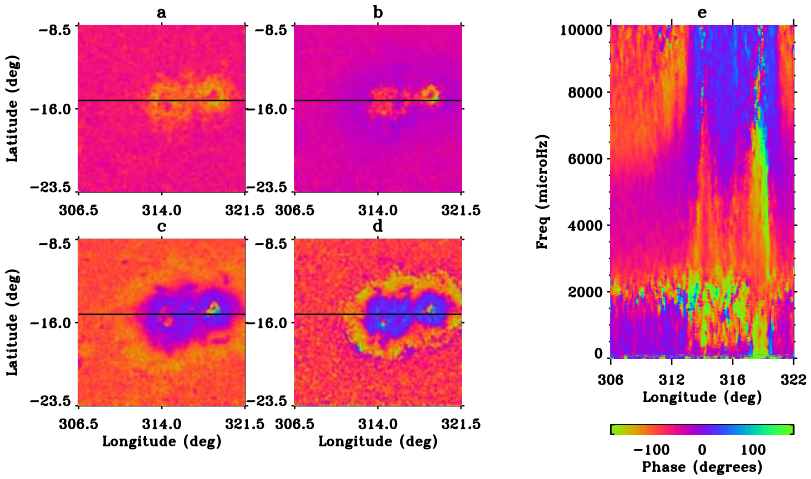

Figure 12. Slices through the AIA 1700/HMI V phase at 3 mHz (a), 5 mHz (b), 7 mHz (c), 9 mHz (d), and in longitude and temporal frequency along the horizontal line shown in panels a-d (e).

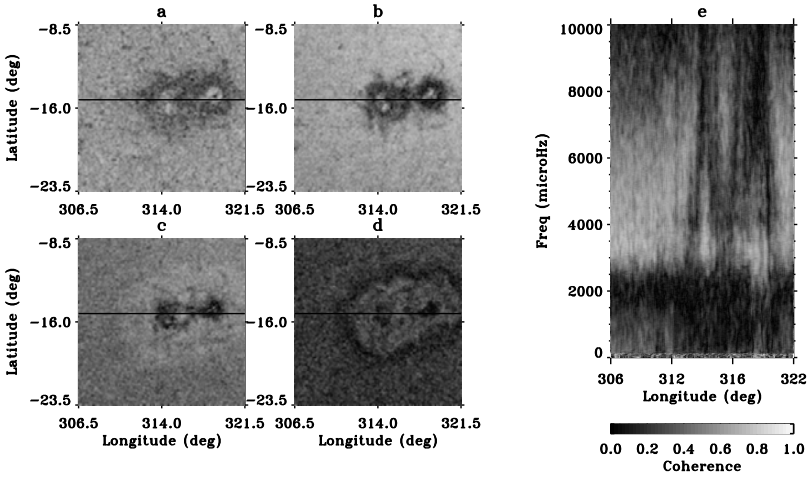

Figure 13. Slices through the AIA 1700/HMI V coherence at 3 mHz (a), 5 mHz (b), 7 mHz (c), 9 mHz (d), and in longitude and temporal frequency along the horizontal line shown in panels a-d (e).

AIA cases, the discontinuity is smaller and the low-frequency behaviour more complicated, with the phase in the plage region heavily disrupted.

While the quiet-Sun phase difference between HMI I and HMI V becomes slowly less negative with increasing frequency, the opposite is true for HMI I_L and the UV bands.

Another interesting feature is that the high-frequency coherence between the HMI V and the UV intensities is higher in the "halo" zone around the active region than in the surrounding quiet Sun; this region (which, as mentioned above, does not correspond to any detectable magnetic fields) also shows a shift in the

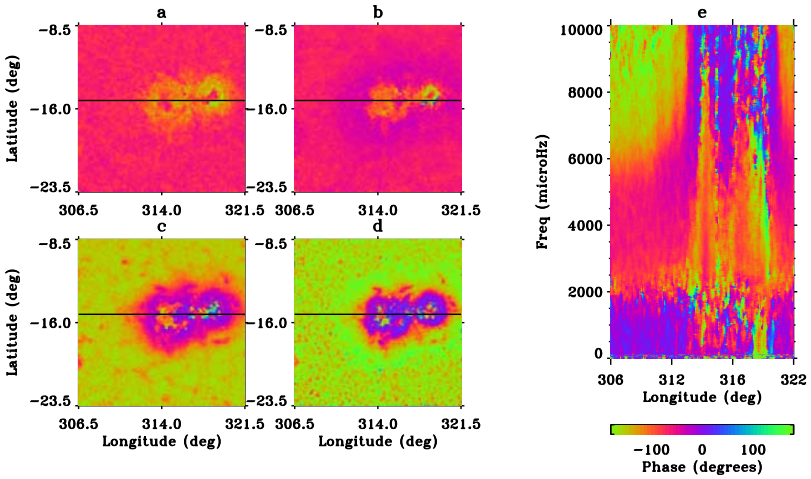

Figure 14. Slices through the AIA 1600/HMI V phase at 3 mHz (a), 5 mHz (b), 7 mHz (c), 9 mHz (d), and in longitude and temporal frequency along the horizontal line shown in panels a-d (e).

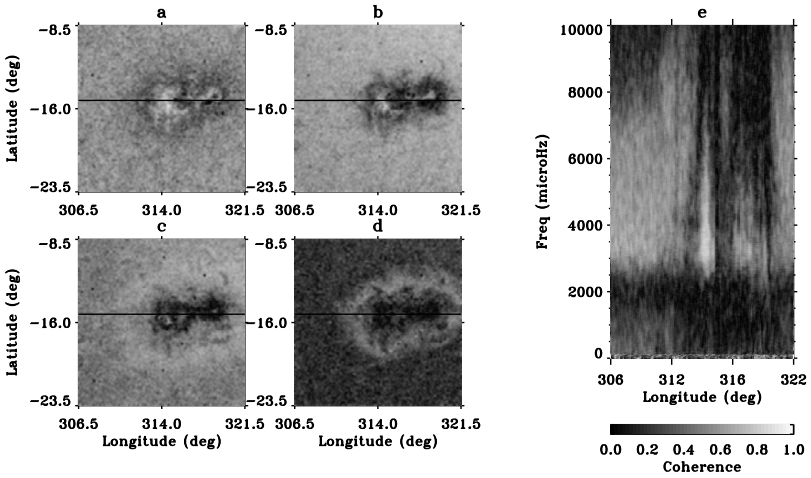

Figure 15. Slices through the AIA 1600/HMI V coherence at 3 mHz (a), 5 mHz (b), 7 mHz (c), 9 mHz (d), and in longitude and temporal frequency along the horizontal line shown in panels a-d (e).

phase between these observables that varies smoothly with distance from the active region, going from a difference of about −100 degrees for the 1700 Å and −160 degrees for the 1600 Å band in quiet Sun far away from the active region at 7 mHz to nearly in-phase within it. While the coherence of HMI V with AIA 1600 and 1700 look very similar at lower frequencies, the 9mHz map shows a different pattern; while for the 1700 band the coherence is weakly enhanced over most of the extended halo region except for the active region core and an external fringe of reduced coherence, for the 1600 band there is a high-coherence fringe surrounding a patch of reduced coherence over the wider active region.

On the other hand, the coherence between HMI V and HMI I_L is reduced in the same region and frequency range, and the phase difference varies from -130 degrees in quiet Sun to -90 degrees in the active region. At 3mHz, conversely, the phase difference between HMI V and both HMI I_L and AIA 1600 and 1700 is more negative within the active region than in quiet Sun. It is curious that the quiet-Sun phase is more negative than that for the AIA bands, as this would seem to imply (if we are dealing with upward-traveling waves) that the HMI I_L is actually probing a higher level of the atmosphere than the UV bands.

6. Discussion

We have examined the acoustic power distribution around an active region in a number of HMI and AIA observables, and the phase and coherence relationships between the intensity observables and the HMI Doppler velocity.

Five-minute power in all observables is suppressed in the sunspot (which is dark at all wavelengths) and also in plage areas (bright in AIA bands and HMI I_L). Above the acoustic cut-off frequency the behaviour is more complicated. Power in HMI I_C is suppressed in the presence of surface fields at all frequencies, while power in HMI V is enhanced in a narrow zone around field concentrations (especially plage) and suppressed in a wider surrounding area; these results are consistent with earlier work using MDI. Power in HMI I_L and the AIA bands is suppressed in areas of surface field but — in contrast to the results of Muglach (2003) — enhanced in an extended area around the active region. In the HMI I_L case, the pattern of narrow halo, encroaching on the region where the five-minute power is suppressed, and surrounding region of suppressed power, seen for the HMI V at 7mHz, is seen instead at 9mHz. For the UV bands, however, this pattern does not appear at any frequency; instead, the halo power fades with increasing frequency and vanishes above about 10mHz while the power suppression remains.

In all cases but HMI I_C, the regions of enhancement and suppression of power appear to move inwards towards the active region at increasing frequency.

The relative phase of the observables is altered around active regions. While the apparently in-phase behaviour of most observables in strong-field areas is associated with low coherence and thus of low significance, there are exceptions to this. In particular, in the 7 mHz frequency band there are areas close to the active region where the AIA 1700 and 1600 bands are both close in phase to the HMI velocity and coherent with it, whereas in the quiet Sun well away from the active region the phase difference is close to 90 degrees and the coherence is lower. This effect is not seen in the HMI I_L, which is otherwise very similar in its behaviour to the UV bands, though there is a phase difference between the two observables.At 9 mHz the 1600 and 1700 Å bands also show qualitatively different behaviour, suggesting that though there may be substantial overlap between the two wavelength bands, the highest-frequency waves are sensing different layers of the atmosphere.

Clearly, within the "halo" zone surrounding the active region the propagation and reflection of the high-frequency waves differs from that over quiet

Sun, whether due to alteration in the height of formation of the observables, thermal changes, or the direct effect of magnetic fields in trapping, scattering or transforming the waves; also, there are qualitative differences between the purely photospheric observables — even at the relatively high formation level of the HMI I_L — and the UV bands.

In general, the higher the observable is formed, the higher the frequency at which the halo of excess power is found, and the more extensive the halo at the lowest frequency at which it appears. It is tempting to interpret these halo effects in terms of spreading magnetic field canopies, as has been suggested, for example, by Moretti *et al.* (2007), but we note that the extent of the high-frequency halo does not exactly match the morphology of the overlying field seen in the EUV images. The size of the halo and the inner and outer regions of suppressed power appear to vary with frequency as well as with the height of formation of the observable used, contracting with increasing frequency. If the patterns of power distribution are related to spreading out of magnetic fields with height, this would imply that the higher-frequency pseudomodes are being reflected or absorbed at lower layers than the lower-frequency ones.

These effects no doubt also influence the changes in the local helioseismic parameters of modes above the acoustic cut-off frequency, seen for example by Howe *et al.* (2004, 2008), which tend to be in the opposite sense from those experienced by modes in the 5-minute range.

Eventually, we hope to carry out multi-wavelength helioseismic analysis using HMI and AIA data together to extract parameters for local and global acoustic spectra. As the results described here demonstrate, any such analysis will need to take into account the effects of active regions on the phase and coherence of the oscillations.

The continuous, high-cadence, full-disk observations of HMI and AIA allow us to study the behaviour of waves in the photosphere and lower chromosphere at a level of detail that has not previously been possible. These observations may help us to improve our understanding of the interaction of waves and magnetic fields in the different layers of the photosphere.

Acknowledgements RH thanks the National Solar Observatory for computing support, and Yvonne Elsworth for useful discussions. SDO data courtesy SDO (NASA) and the AIA and HMI consortia. This work was partly supported by NASA grant NNH12AT11I to NSO. This research has made use of NASA's Astrophysics Data System.

References

Barban, C., Hill, F., Kras, S.: 2004, *Astrophys. J.* **602**, 516. doi:10.1086/380833.

Braun, D.C., Lindsey, C., Fan, Y., Jefferies, S.M.: 1992, *Astrophys. J.* **392**, 739. doi:10.1086/171477.

Brown, T.M., Bogdan, T.J., Lites, B.W., Thomas, J.H.: 1992, *Astrophys. J.* **394**, L65. doi:10.1086/186473.

Deubner, F.-L., Fleck, B., Marmolino, C., Severino, G.: 1990, *Astron. Astrophys.* **236**, 509.

Deubner, F.-L., Fleck, B., Schmitz, F., Straus, T.: 1992, *Astron. Astrophys.* **266**, 560.

Elsworth, Y., Howe, R., Isaak, G.R., McLeod, C.P., Miller, B.A., New, R., Speake, C.C., Wheeler, S.J.: 1994, *Mon. Not. R. Astr. Soc.* **269**, 529.

Finsterle, W., Jefferies, S.M., Cacciani, A., Rapex, P., Giebink, C., Knox, A., Dimartino, V.: 2004, *Solar Phys.* **220**, 317. doi:10.1023/B:SOLA.0000031397.73790.7b.

Fleck, B., Couvidat, S., Straus, T.: 2011, *Solar Phys.* **271**, 27. doi:10.1007/s11207-011-9783-9.

Fossum, A., Carlsson, M.: 2005, *Astrophys. J.* **625**, 556. doi:10.1086/429614.

Hill, F., Ladenkov, O., Ehgamberdiev, S., Chou, D.-Y.: 2001, In: A. Wilson & P. L. Pallé (ed.) *SOHO 10/GONG 2000 Workshop: Helio- and Asteroseismology at the Dawn of the Millennium*, *ESA Special Publication* **464**, 219.

Howe, R., Komm, R.W., Hill, F., Haber, D.A., Hindman, B.W.: 2004, *Astrophys. J.* **608**, 562. doi:10.1086/392525.

Howe, R., Haber, D.A., Hindman, B.W., Komm, R., Hill, F., Gonzalez Hernandez, I.: 2008, In: R. Howe, R. W. Komm, K. S. Balasubramaniam, & G. J. D. Petrie (ed.) *Subsurface and Atmospheric Influences on Solar Activity*, *Astronomical Society of the Pacific Conference Series* **383**, 305.

Howe, R., Hill, F., Komm, R., Broomhall, A., Chaplin, W.J., Elsworth, Y.: 2011, *Journal of Physics Conference Series* **271**(1), 012058. doi:10.1088/1742-6596/271/1/012058.

Jain, R., Haber, D.: 2002, *Astron. Astrophys.* **387**, 1092. doi:10.1051/0004-6361:20020310.

Jiménez, A., Roca Cortés, T., Severino, G., Marmolino, C.: 1999, *Astrophys. J.* **525**, 1042. doi:10.1086/307925.

Judge, P.G., Tarbell, T.D., Wilhelm, K.: 2001, *Astrophys. J.* **554**, 424. doi:10.1086/321383.

Krijger, J.M., Rutten, R.J., Lites, B.W., Straus, T., Shine, R.A., Tarbell, T.D.: 2001, *Astron. Astrophys.* **379**, 1052. doi:10.1051/0004-6361:20011320.

Moretti, P.F., Jefferies, S.M., Armstrong, J.D., McIntosh, S.W.: 2007, *Astron. Astrophys.* **471**, 961. doi:10.1051/0004-6361:20077247.

Muglach, K.: 2003, *Astron. Astrophys.* **401**, 685. doi:10.1051/0004-6361:20021901.

Norton, A.A., Graham, J.P., Ulrich, R.K., Schou, J., Tomczyk, S., Liu, Y., Lites, B.W., López Ariste, A., Bush, R.I., Socas-Navarro, H., Scherrer, P.H.: 2006, *Solar Phys.* **239**, 69. doi:10.1007/s11207-006-0279-y.

Scherrer, P.H., Bogart, R.S., Bush, R.I., Hoeksema, J.T., Kosovichev, A.G., Schou, J., Rosenberg, W., Springer, L., Tarbell, T.D., Title, A., Wolfson, C.J., Zayer, I., MDI Engineering Team: 1995, *Solar Phys.* **162**, 129.

Schunker, H., Braun, D.C.: 2011, *Solar Phys.* **268**, 349. doi:10.1007/s11207-010-9550-3.

Severino, G., Magrì, M., Oliviero, M., Straus, T., Jefferies, S.M.: 2001, *Astrophys. J.* **561**, 444. doi:10.1086/323243.

Staiger, J.: 1985,. PhD thesis, Thesis, University of Freiburg i. Br., (1985).